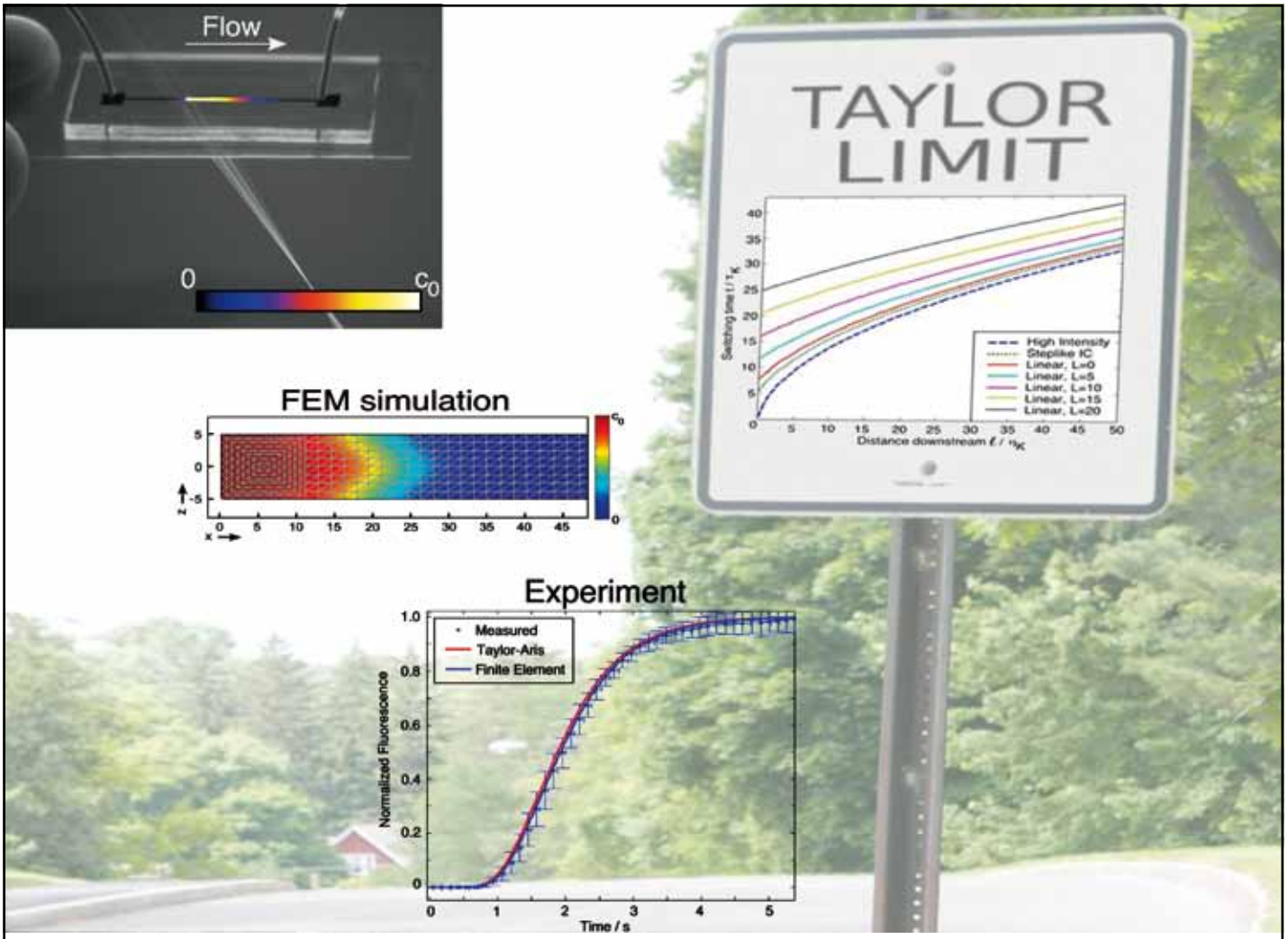

Featuring research from the Chemotaxis and Actin-based Motility group of Eberhard Bodenschatz at the Max Planck Institute for Dynamics and Self-Organization.

Title: Rapid switching of chemical signals in microfluidic devices

Dispersion of the concentration front imposes a speed limit on how quickly a chemical signal can be applied in a microfluidic device. We investigate this limit using Taylor–Aris theory and finite element simulations.

As featured in:

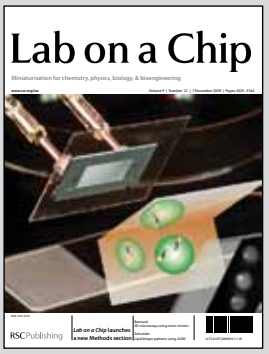

See Beta *et al.*, *Lab Chip*, 2009, **9**, 3059–3065.

RSC Publishing

www.rsc.org

Registered Charity Number 207890

Rapid switching of chemical signals in microfluidic devices†

Albert J. Bae,[ab] Carsten Beta*[ac] and Eberhard Bodenschatz[ab]

Received 18th March 2009, Accepted 15th June 2009
First published as an Advance Article on the web 3rd July 2009
DOI: 10.1039/b905521e

We present an analysis of concentration switching times in microfluidic devices. The limits of rapid switching are analyzed based on the theory of dispersion by Taylor and Aris and compared to both experiments and numerical simulations. We focus on switching times obtained by photo-activation of caged compounds in a micro-flow (flow photolysis). The performance of flow photolysis is compared to other switching techniques. A flow chart is provided to facilitate the application of our theoretical analysis to microfluidic switching devices.

1 Introduction

Over the past decade, microfluidics was established as a highly versatile experimental platform for the life sciences.[4,6] Benefits include rapid and inexpensive fabrication, versatile design, biocompatible materials, and small sampling volumes. Complex tasks, like the polymerase chain reaction[21] or the screening for conditions of protein crystallization,[13] can be miniaturized and open promising opportunities for large scale integration.[28]

In particular, microfluidics provides us with a powerful environment for well-controlled live cell experiments. For example, microfluidic devices have been successfully applied to generate chemical gradients for the investigation of directed cell growth[7] and studies of chemotaxis in neutrophils,[16,14] *Dictyostelium discoideum*,[24] and carcinoma cells.[23,25] Moreover, they offer unique possibilities for single cell experiments with high spatial resolution.[26] Today, microfluidic applications range from individualized setups for the specific handling and addressing of single cells to high throughput cellomics platforms.[1]

Most of these devices expose cells to temporally static chemical signals. However, the live cell response to an extracellular cue is a dynamical process. The characteristic response times of many receptor mediated signaling pathways is on the order of 1 s.[11] Thus, experimental tools are required to expose single cells to stimuli with subsecond temporal resolution. Recently, microfluidic techniques have been developed to generate time-dependent chemical signals. They are mostly based on one of the following principles: (*i*) *Valve-mediated switching;* a valve system is used to switch between flows of different concentration. For example in Ref. 15, temporally changing gradient signals were generated using valve-mediated switching. (*ii*) *Interface shifting;* by changing the flow speed at the fluid inlets, the interface between regions of different concentration can be swept across a cell, changing its chemical surroundings.[30,18,17] (*iii*) *Light-induced switching;* rapid switching of chemical signals can be achieved by the use of photo-activatable compounds, a technique termed *flow photolysis*.[5] It is based on the following principle. A physiologically inert caged compound is activated in a microflow by light induced cleavage of a photoliable bond. The uncaged compound is carried downstream, where it is delivered to a target for stimulation, see Fig. 1. Most microfluidic switching devices can be grouped into one of these major categories. Besides, a number of more exotic switching techniques has been designed, for example, the physical movement of a cell through a nonuniform concentration field.[22] The latter will not be further considered here.

In this article, we will analyze the temporal resolution in switching devices of type (*i*)–(*iii*). This resolution is limited by dispersion resulting from the interaction between convective and diffusive transport. The further a concentration front travels down a microfluidic channel, the more it will be blurred by dispersion. In Section 2, we summarize the theory of Taylor[27] and Aris[2] that quantitatively describes this phenomenon. Temporal resolution can be increased by raising the flow speed. However, live cell experiments impose strict upper limits on the speed of fluid flow in microfluidic channels. If the flow speed is increased beyond a critical threshold, the resulting shear stress on a cell may induce mechanotactic responses,[8,12,20] or even wash adherent cells off the substrate.[9] Given a physiologically relevant flow speed, what are the limits dispersion imposes on the temporal resolution of a chemical signal we deliver to a cell?

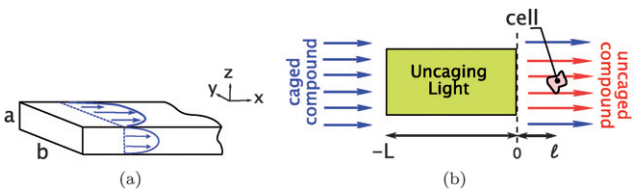

Fig. 1 (a) Geometry of a rectangular microfluidic flow chamber. The reference frame is chosen such that x increases in the direction of fluid flow, y increases across the channel, and z points vertically up the channel. (b) Schematic top view of a photo-uncaging setup (x–y plane). The area illuminated by the uncaging light source is indicated in yellow and extends over a length of L in flow direction. For stimulation the cell is placed a distance l downstream of the illuminated region. Fluid flow runs from left to right.

[a]*Max Planck Institute for Dynamics and Self-Organization, Am Fassberg 11, 37077 Göttingen, Germany*
[b]*Laboratory of Atomic and Solid State Physics, Department of Physics, Cornell University, Ithaca, NY, 14853, USA*
[c]*Institute of Physics und Astronomy, University of Potsdam, Karl-Liebknecht-Str. 24/25, 14476 Potsdam-Golm, Germany*
† Electronic supplementary information (ESI) available: Supplementary notes on Taylor–Aris dispersion. See DOI: 10.1039/b905521e

From a theoretical standpoint, the flow photolysis system is the most general of the three switching techniques. Therefore, in Section 3, we perform a detailed analysis of the theoretical limits of rapid switching in flow photolysis devices, *i.e.* in systems of type (*iii*). Furthermore, a set of experimental data is provided to test our theoretical predictions on the flow photolysis method. In Section 4, we extend the theory of switching to devices of type (*i*) and (*ii*). In doing so, we demonstrate that setups of type (*iii*) are optimally suited to reduce the switching time; *i.e.*, the highest temporal resolution can be expected for devices using the flow photolysis approach.

2 Taylor–Aris theory

Let us consider a micro-channel of height a and width b. Our reference frame is chosen such that x increases in the direction of flow (from left to right), y increases across the channel, and z points vertically from the bottom to the top of the channel, see Fig. 1(a). We assume that a solute is transported by the flow. The evolution of its concentration is given by the convection–diffusion equation,

$$\frac{\partial c}{\partial t} + \mathbf{u}\cdot\nabla c = D\nabla^2 c + s \tag{1}$$

where c is the concentration of the solute, D its diffusion coefficient, and $\mathbf{u}$ is the flow velocity. The term s denotes a source of the solute concentration c and can be a function of space and time. The cell that will be stimulated is located a distance l downstream of the source. We assume that adhesion of the cell to the channel wall is sufficiently strong to withstand moderate shear stress exerted by the microflow.[9] For non-adhesive or weakly adhesive cell types this can be achieved by an additional adhesive coating of the channel walls.

We assume that the length of the channel in the flow direction is much larger than all other relevant length scales. The parameters that characterize the flow problem are thus the height a and the width b of the micro-channel, the distance l that the cell is placed downstream of the source, the diffusion coefficient D of the solute, and the average flow velocity $\bar{u}$. The ratios $D/\bar{u}$ and $D/\bar{u}^2$ define the diffusive length and time scales. Based on this length scale, we can construct three dimensionless Péclet numbers, $Pe = \bar{u}l/D$, $Pe_a = \bar{u}a/D$, and $Pe_b = \bar{u}b/D$. If parameters are changed such that the Péclet numbers remain constant, both the flow and the concentration profiles scale.

For wide and shallow microfluidic channels (large aspect ratio $\gamma = b/a$), far from the sidewalls, the flow profile is independent of the y coordinate. With respect to the height coordinate z, the flow profile takes on a parabolic shape. Assuming that the concentration varies slowly in the y direction, the problem can be analyzed in two dimensions; *i.e.*, the role of Pe_b is negligible. The switching time predicted under these assumptions should provide a lower limit in geometries where these conditions are not fulfilled.

The flow problem may be further simplified to one dimension, if the Taylor–Aris theory of dispersion can be applied. In his seminal work,[27] Taylor described how an initial plug of diffusible solute spreads in a laminar fluid flow through a small-bore cylindrical tube. In the tube, the flow velocity profile is parabolic. In absence of diffusion, the concentration profile would reflect the flow profile. As time evolves, axial spreading of the plug occurs: the solute next to the boundaries does not move, whereas the center of the plug is convected at twice the mean flow velocity. If diffusion is taken into account, the convective transport of the solute will be superposed with a diffusive spreading of the concentration profile. For large diffusivity or small cross section of the tube, diffusion in radial direction prevents the formation of a parabolic concentration profile. Instead, a compact plug profile is maintained; *i.e.*, the concentration does not depend on the radial coordinate. Only axial dispersion about the center of the plug occurs as it is convected down the tube.

Taylor showed that the center of the plug moves with the mean flow velocity, while diffusive spreading of the plug about its center can be described by an effective diffusion coefficient. Aris[2] generalized this result for tubes of arbitrary cross section. He showed that the effective axial diffusion of a plug of solute is given by

$$K = D(1 + \kappa Pe_a{}^2) \tag{2}$$

where the geometrical factor κ depends on the shape of the tube cross section. For our wide and shallow rectangular geometry, $\kappa = 1/210$.[3,10]

We can apply Taylor–Aris theory if diffusive transport across the channel height a is much faster than convective transport over the length l; *i.e.*, $a^2/(4\pi^2 D) \ll l/\bar{u}$.† In terms of the Péclet numbers,

$$Pe_a^2 \ll 4\pi^2 Pe \tag{3}$$

When this condition is satisfied, diffusion will remove vertical distortions of the concentration profile due to the parabolic flow profile. In the Section 3.4, we will examine this condition in more detail.

3 Rapid switching by flow photolysis

Based on Taylor–Aris theory, we will perform a detailed analysis of the concentration switching times that can be obtained in flow photolysis setups. In Section 4, these results will be compared to the temporal resolution in other live cell stimulation devices.

3.1 Device geometry and governing equations

Flow photolysis is a microfluidics-based approach for single cell stimulation with high spatiotemporal resolution. Here, we will briefly introduce the underlying principle. For more details, the reader is referred to Ref. 5. The main idea of flow photolysis is summarized in Fig. 1(b). A flow is established in a microfluidic channel that carries a physiologically inert caged compound of initial concentration c_0. In the flow, a rectangular region, of length L in flow direction, is illuminated with short wavelength light (uncaging region). A distance l downstream of the uncaging region, the target for chemical stimulation — in most cases a living cell — is placed. The wavelength of the uncaging light source is chosen such that it cleaves the photoliable bond between the caging group and the physiologically active part of the caged compound. The released active substance is then carried across the cell downstream by the fluid flow.

In many cases, the caging group is small compared to the physiologically active part of the caged compound, so we may approximate the diffusion coefficients of the caged and uncaged compound to be equal.† The concentration c of uncaged material then evolves according to

$$\frac{\partial c}{\partial t} = -\bar{u}\frac{\partial c}{\partial x} + K\frac{\partial^2 c}{\partial x^2} + (c_0 - c)f(x,t) \quad (4)$$

with the initial condition $c(x, 0) = 0$. The photochemical release of c in the uncaging region is described by the function $f(x, t)$,

$$f(x,t) = \begin{cases} \sigma\phi I & \text{for } -L \le x \le 0 \quad \text{and} \quad t > 0 \\ 0 & \text{elsewhere,} \end{cases}$$

where I is the light intensity, σ the absorption cross-section, and ϕ the quantum yield of the cage. In general, the time-scale for the cleavage of the photoliable bond is fast compared to the other time scales involved in the problem, and therefore has not been included in our description.

Let us introduce the dispersive length scale $\eta_K = K/\bar{u}$, the dispersive time scale $\tau_K = K/\bar{u}^2$, the photolysis time scale $\tau_p = (\sigma\phi I)^{-1}$, and the residence time $\tau_r = L/\bar{u}$. Then using units of η_K for x and τ_K for t, we can rewrite Eq. (4) as

$$\frac{\partial c}{\partial t} = -\frac{\partial c}{\partial x} + \frac{\partial^2 c}{\partial x^2} + (c_0 - c)f(x,t) \quad (5)$$

with the uncaging light source described by

$$f(x,t) = \begin{cases} \tau_K/\tau_p & \text{for } -L/\eta_K \le x \le 0 \quad \text{and} \quad t > 0 \\ 0 & \text{elsewhere.} \end{cases}$$

3.2 Steady state solution

If the uncaging light source is switched on, photo-cleavage of the caged substance is initiated and the released compound is transported downstream by the flow. At the same time, new uncaged substance is convected into the uncaging region. After a short time, a stationary state is reached that is characterized by a continuous release of uncaged substance from the uncaging area and a constant concentration profile downstream of this region. Let us consider the two limiting cases of low and high uncaging light intensities.†

Linear regime. For low light intensities, such that $\tau_p \gg \tau_K$, the concentration to the right of the uncaging region is

$$c(x > 0) = c_0(1 - e^{-\tau_r/\tau_p}) \quad (6)$$

Under the additional condition that the photolysis time-scale is greater than the residence time, $\tau_p \gg \tau_r$, we obtain

$$c\,(x > 0) = \frac{c_0\tau_r}{\tau_p} = \frac{c_0\sigma\phi IL}{\bar{u}} \quad (7)$$

In Ref. 5, we demonstrated that the concentration profile of the uncaged substance downstream of the illuminated region can be modified by changing the shape of the uncaging area. In the regime described by Eq. (7), the extension of the uncaging area in the flow direction (x) is linearly mapped to the amount of uncaged substance.

Saturating regime. For high uncaging light intensities, $\tau_p \ll \tau_K$, we obtain $c = c_0$ for $x > 0$. All of the caged substance is photocleaved immediately as the material enters the uncaging region. In this limit, a mapping of the light source geometry on the concentration profile is not possible.

3.3 Time dependent solution

We will now turn to the dynamics of the switching event. For both the linear and the stationary regime, the derivations of the time dependent solutions of Eq. (5) are presented in the ESI.†

Linear regime. When $\tau_p \gg \tau_K$ and $\tau_p \gg \tau_r$, only a small fraction of the caged substance is released, $c \ll c_0$. From the linear regime solution of Eq. (5)†, we obtain the switching time, which we define as the time interval for the concentration $c(l, t)$ to rise from 5% to 95% of its final value. The switching time increases with increasing residence time $L/\bar{u}$. In Fig. 2, the switching time in the linear regime for $L = 0$, 5, 10, 15, and 20 η_K is shown by the red, light blue, purple, yellow, and black lines.

Saturating regime. When $\tau_p \ll \tau_K$, all caged substance that passes the light source is released immediately. We solve Eq. (5) in the saturating regime.† The switching time, as a function of the distance l, is shown by the dashed blue line in Fig. 2. Note that switching in the linear regime is always slower than in the saturating regime. Yet, for generating spatially varying concentration profiles, it is often desirable to operate in the linear regime.

3.4 Limits of the Taylor–Aris prediction

To explore the limits of the theoretical predictions presented above, we have conducted photo-activation measurements with

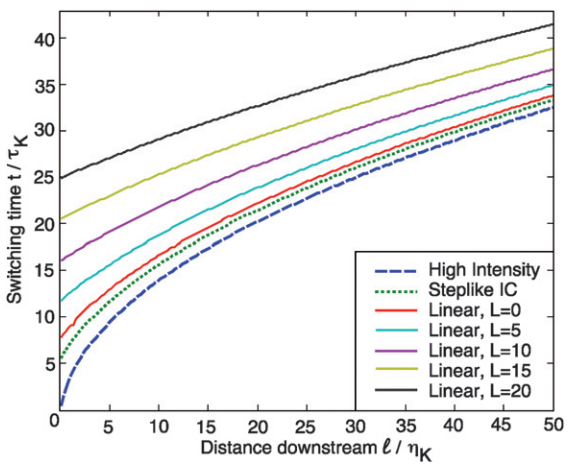

Fig. 2 Switching time as a function of the distance downstream of the source. The switching time is defined as the time interval for the concentration to rise from 5% to 95% of its final value. The dashed blue line shows switching in a flow photolysis device in the saturating regime (for high light intensities). The dynamics of valve-mediated switching and interface shifting, *i.e.*, for a step-like initial condition, is displayed with the green dashed line. The red, light blue, purple, yellow, and black curves show switching times in a flow photolysis device that is operated in the linear regime (for low light intensities) for different uncaging region lengths, $L = 0$, 5, 10, 15, and 20 η_K.

a caged dye and performed numerical finite element simulations of the flow photolysis setup.

Experimental results. We used a large aspect ratio microchannel of height $a = 26$ μm and width $b = 500$ μm. A continuous fluid flow, carrying a 10 μM solution of dextran conjugated 4,5-dimethoxy-2-nitrobenzyl (DMNB)-caged fluorescein, $D = 267$ μm^2/s,† was established in the channel. Switching events were initiated by a 405 nm laser uncaging light source. We measured the increase of fluorescence intensity a distance l downstream of the uncaging region, near the bottom of the channel. Two sets of measurements were acquired at different distances l and different flow velocities $\bar{u}$. In both cases, the width of the uncaging region is negligible compared to the length scale l; *i.e.*, $L \ll l$.

The first measurement set was taken at a distance $l = 86$ μm downstream of the uncaging region. The flow velocity was $\bar{u} = 43$ μm/s, so the corresponding Péclet numbers were $Pe_a = 4.2$ and $Pe = 14$. In this case, $Pe_a^2/Pe = 1.3 \ll 4\pi^2$, satisfies the Taylor condition (3). Consequently, in Fig. 3(a), we see excellent agreement between the experimental results and the Taylor–Aris prediction. The rise in fluorescence intensity, which reflects the concentration of uncaged material, is shown as blue points. The red line displays the theoretical prediction according to Taylor and Aris.

The second measurement set was taken at $l = 25$ μm with flow velocity $\bar{u} = 104$ μm/s. The corresponding Péclet numbers were $Pe_a = 10$ and $Pe = 9.8$. In this case, the ratio $Pe_a{}^2/Pe = 11$ only weakly satisfies the Taylor condition (3). The switching event for this choice of parameters is displayed in Fig. 3(b). A clear discrepancy between the prediction and the experimental result is observed. To further investigate the accuracy of Taylor–Aris theory, we have performed numerical simulations of the photolysis induced switching events using the finite element method (FEM).

Numerical simulations. We solved the convection–diffusion equation (1) in two dimensions (x, z) for the photo-uncaging geometry used in our experiments. The solid blue lines in Figs. 3(a) and 3(b) display the numerical results. They correspond to the values of Pe and Pe_a that describe the experiments. In both cases, the agreement between the FEM solution and experiment is excellent.

We extended these simulations and obtained a systematic set of data to characterize deviations from Taylor–Aris theory as

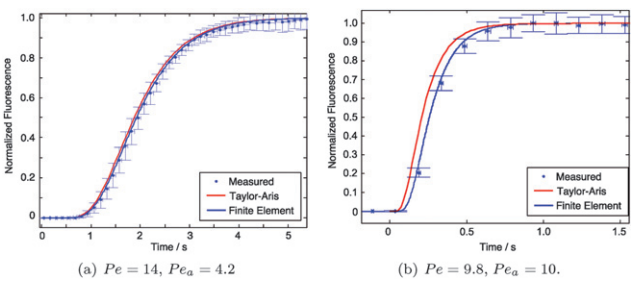

Fig. 3 Concentration switching in the flow photolysis device. Comparison between experimental data (blue points), numerical finite element simulation (blue line), and analytic prediction according to the Taylor–Aris dispersion theory.

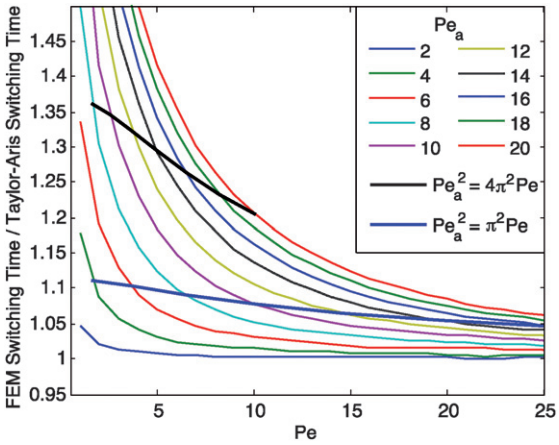

Fig. 4 Comparison of switching times obtained from finite element simulations and Taylor–Aris theory. Relative switching times are shown as a function of Pe for different values of Pe_a. The bold lines correspond to a constant ratio of $Pe_a{}^2 = 4\pi^2 Pe$ (black) and $\pi^2 Pe$ (blue).

a function of the Péclet numbers Pe and Pe_a. In Fig. 4, we summarize the results in terms of the relative switching time: the ratio of the switching time, taken on the bottom boundary of the FEM solution, and the switching time predicted by the one dimensional Taylor–Aris theory. For the two experimental cases discussed above Taylor–Aris theory underestimates the switching time by 1% in the first ($Pe_a = 4.2$, $Pe = 14$) and by 8% in the second case ($Pe_a = 10$, $Pe = 9.8$). In addition, two examples of constant ratio $Pe_a{}^2/Pe$ are displayed by the bold black and blue lines. They correspond to $Pe_a{}^2 = 4\pi^2 Pe$ and $Pe_a{}^2 = \pi^2 Pe$. It can be seen that the Taylor–Aris theory remains accurate within about 10% by choosing $Pe_a{}^2 = \pi^2 Pe$.

Even in cases where the switching times predicted by Taylor–Aris theory are not particularly accurate, they still provide a useful lower bound — in Fig. 4, all the curves remain above unity. This can be understood by a simple consideration: the Taylor–Aris approximation assumes that vertical diffusion removes the dependence of the concentration on the z coordinate. If this approximation is not fulfilled, the concentration profile reflects the parabolic flow profile. Compared to the Taylor–Aris limit, the concentration front now advances faster in the center and slower at the top and bottom walls of the channel, where the cells are placed for stimulation.

4 Extension of theory to other techniques

In this section, we extend the theory to *valve-mediated switching* and *interface sweeping*. We compare the performance of these techniques to flow photolysis. Examples are given in Table 1.

Valve-mediated switching

Let us first consider microfluidic systems, where the chemical agent is introduced by opening a valve. Similar to the flow photolysis setup, the dynamics of the solute will be described by Eq. (5). Here, $x = 0$ is the location of the valve that introduces the agent. Since there is no uncaging light, we set $I = 0$. Rather, we have an initial condition $c(x, 0) = c_0 H(-x)$, where H is the

Table 1 The wall shear stress τ and theoretical switching time t_{switch} for representative parameters a, l, $\bar{u}$, and D corresponding to (1) the flow photolysis method, (2a)–(3a) valve mediated switching,[15,14] and (4a) interface sweeping.[19] Examples (2b)–(4b) compare the performance of these devices when we match the diffusivity and shear stress to example (1)

Example	a (μm)	l (μm)	$\bar{u}$ (μm/s)	D (μm²/s)	τ (mPa)	t_{switch} (s)
1	26	25	104	267	24	0.4
2a	100	1.8×10^3	370	425	22	3.5
3a	25	250	200	425	48	0.7
4a	50	10^3	3×10^4	270	3.6×10^3	0.1
2b	100	1.8×10^3	400	267	24	4.2
3b	25	250	100	267	24	1.4
4b	50	10^3	200	267	24	2.3

Heaviside function. Again, expressing x and t in units of η_K and τ_K, we obtain the solution†

$$c(x,t) = \frac{c_0}{2}\,\mathrm{erfc}\left(\frac{x-t}{2\sqrt{t}}\right) \tag{8}$$

The resulting dependence of the switching time on l is displayed in Fig. 2 by the green dotted line. The rise time for the valve-mediated system is always longer than for the photolysis device operating in the saturating regime.

A microfluidic system that implements rapid switching of concentration gradients using valves was developed by Irimia *et al.*[15] Based on their flow parameters, we can estimate the Péclet numbers in their device to be $Pe_a = 87$ and $Pe = 1520$. Taylor–Aris theory is applicable, since $Pe_a^2/Pe = 5.0$. Based on Eq. (8), *i.e.* Fig. 2, we calculate a switching time of 3.5 s, which is in good agreement with their reported switching time of approximately 4 s.†

Interface sweeping

The second major class of microfluidic switching devices employs pressure induced changes in flow speed to shift the interface between regions of different concentration.

As the prototypical design of such a device, a Y-junction can be considered. Via the Y-junction, two fluids of different concentration are injected into the rectangular main channel. An interface forms between the two fluids. The location of this interface in the channel depends directly on the ratio of the injection flow rates. If a cell is placed in the center of the channel, we may sweep the interface across the cell by adjusting the flow rates and thus expose the cell to a switching of ambient chemical concentrations.

What are the short time limits of switching that can be reached in such devices? Kuczenski *et al.* have experimentally characterized laminar interface shifting in a microfluidic setup, using ink and water to visualize the interface.[18] They obtained switching times of less than 0.1 s, which was their measurement resolution. These extremely quick events were achieved by using an average flow velocity of $\bar{u} \approx 2 \times 10^5$ μm/s—three orders of magnitude higher than the flow velocities that we used in the experiments presented in Section 3.4. We must note that, for most live cell experiments, the flow induced wall shear stress imposes upper limits on the flow velocities that we can use. Detailed studies of shear induced cell detachment have been performed, *e.g.*, for the social amoeba *Dictyostelium discoideum*, a strongly adherent chemotactic microorganism. It was found that half of a population of adherent *Dictyostelium* cells are washed away at a shear stress of $\tau_{1/2} = 2.4$ Pa.[9] The shear stress in the experiments by Kuczenski *et al.* was $\tau \approx 30$ Pa, *i.e.*, ten times higher than the critical detachment value reported in Ref. 9. Furthermore, it has been shown that at shear stresses around 1 Pa, living cells may exhibit mechanotactic responses.[8,12,20] Therefore, flow speeds in the range that was used in Ref. 18 are not suitable for many live cell experiments. In a recent publication, Ref. 19, Kuckzenski *et al.* have applied their approach to fibroblast stimulation experiments using strongly reduced flow speeds.

Let us consider the limits on fast concentration switching in such devices using the framework of Taylor–Aris theory. Ideally, the inlet pressures that drive the flow and determine the position of the interface can be adjusted immediately. Upon a change in the ratio of inlet pressures, the velocity field changes instantaneously, compared to the time it takes for the material to be convectively displaced. This is shown in Fig. 5. The solid gray line shows the interface that forms when the ratio of flow rates between the top and bottom inlets of the channel is $q_1/q_2 = 3$. If this ratio is changed to $q_1/q_2 = 1/3$, a new velocity field emerges, the streamlines of which are illustrated as blue curves. In Fig. 5, the resulting time evolution of the interface is shown by red lines that are evenly spaced in time. We note that the interface is shifting to its new position in the form of an oblique traveling wave. The wavefront propagates with the average downstream flow velocity, and as it moves, it undergoes dispersion. Therefore, Taylor–Aris theory can be applied to estimate the switching times at various positions in the channel. In particular, in cases where one of the input flow rates is switched to zero, the method of interface shifting becomes identical to valve-based switching. Thus, the same general limits apply for the switching time that were discussed for valve-based switching. Consequently, also in this case, flow photolysis provides the faster switching events.

5 Conclusion

Dispersion provides a limit on the temporal resolution of chemical signals we can provide cells in a microfluidic device. In this article, we presented a detailed analysis of switching times in

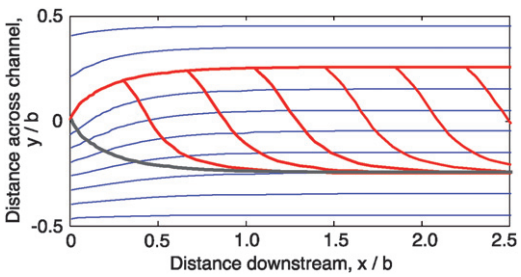

Fig. 5 Interface sweeping. The initial interface is shown as a solid gray line and results from a ratio of inlet flow rates of $q_1/q_2 = 3$. The blue lines show the streamlines after switching of the inlet flow rates to a ratio of $q_1/q_2 = 1/3$. The red lines display the interface evolution following the switch in the ratio of inlet flow rates at evenly spaced points in time.

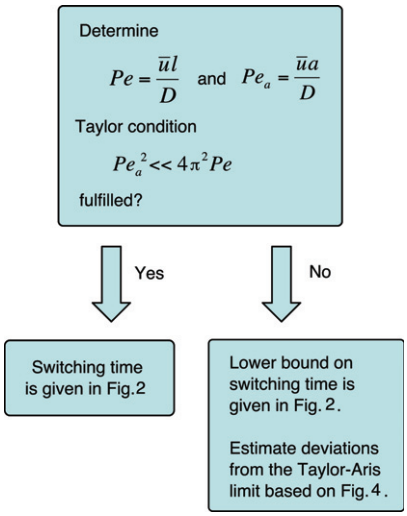

Fig. 6 Flow chart application scheme to estimate the switching time in a microfluidic device based on the channel geometry and the flow parameters.

the microfluidic flow photolysis setup. The limits of rapid concentration switching were analyzed based on theoretical predictions by Taylor and Aris and compared to experimental and numerical results. We discussed our findings in the context of other microfluidic switching techniques like valve-based switching and interface sweeping. We showed that the highest temporal resolution is achieved in flow photolysis devices.

To facilitate the application of our theoretical results for the non-specialist user, we summarize our findings in a brief application protocol. On the basis of this protocol, concentration switching times in microfluidic devices can be estimated.

• Calculate the Péclet numbers $Pe = \bar{u}l/D$ and $Pe_a = \bar{u}a/D$ and check whether the Taylor condition (3) is fulfilled.

• If condition (3) is satisfied, the switching time can be determined from Fig. 2, or for more accuracy, the code in the electronic supplementray material may be used.

• If condition (3) is not satisfied, Fig. 2 gives a lower bound on the true switching time. The deviation from this lower bound may be estimated with Fig. 4.

The protocol is summarized in terms of a flow chart in Fig. 6. Note that in Fig. 2, the switching time and the distance downstream of the chemical source are given in units of $\tau_K = K/\bar{u}^2$ and $\eta_K = K/\bar{u}$, respectively. The corresponding numbers from a specific experimental setup will be given in seconds and meters and thus have to be converted before they may be used in conjunction with Fig. 2. This conversion requires that the effective diffusion coefficient K is determined on the basis of the diffusion constant D of the solute and the Péclet number Pe, see Eq. (2).

6 Materials and methods

Experimental setup

The experiments described in Section 3.4 were performed with the flow photolysis setup described by Beta *et al.*[5] We fabricated microfluidic channels in polydimethylsiloxane (PDMS; Sylgard 184 Dow Corning) using standard soft lithography techniques.[29] The height and width of the microchannel were $a = 26$ μm and $b = 500$ μm, respectively. The length of the channel was 3.0 cm. A 500 μL syringe (1750 TTLX, Hamilton) supplied the channel with a 10 μM solution of 4,5-dimethoxy-2-nitrobenzyl (DMNB)-caged fluorescein (dextran conjugate, 3000 MW, Invitrogen). A constant fluid flow through the channel was maintained by a precision syringe pump (PHD 2000, Harvard Apparatus).

Imaging was performed with a laser scanning confocal microscope (Fluoview FV1000, Olympus) that was equipped with a separate scanner to move a photoactivation laser spot independently of the imaging lasers inside the field of view. A 25 mW, 405 nm laser (FV5-LD405, Olympus) was used to photoactivate (uncage) the fluorescein. The uncaged fluorescein was detected by laser excitation at 488 nm with the standard imaging system of the confocal microscope.

Two sets of measurements were taken, (a) in a regime where the Taylor condition (3) is well satisfied and (b) in a regime where the condition is poorly satisfied. In (a), we set the average flow speed to $\bar{u} = 43$ μm/s. A 40× objective was used. The uncaging line was 79 μm long and the fluorescence intensity of the released dye was measured inside a 13 μm × 13 μm detection region that was located 86 μm downstream. In (b), the average flow speed was $\bar{u} = 104$ μm/s. Imaging was performed with a 60× objective. The uncaging laser scanned a 50 μm line perpendicular to the flow direction. The 8 μm × 8 μm measurement region was located 25 μm downstream from the center of the uncaging region.

For each set of measurements, we imaged far from the side walls, near the center of the device. The focal plane was chosen close to the bottom glass wall of the channel. To obtain good statistics, we took ten measurements of the switching event, *i.e.* the rise in fluorescence intensity following initiation of the uncaging laser, averaged over the measurement window. The time when the photo-activation laser is turned on is denoted as $t = 0$. The imaging frame rate was nominally 10 Hz. The results are displayed in Fig. 3. The vertical error bars correspond to the standard deviation in average intensity over the ten time series measurements. The horizontal error bars show the standard deviation in the times at which each measurement was taken.

Numerics

We solved the convection–diffusion equation (1) in two dimensions (x, z) for Péclet numbers of $Pe_a = 2, 4, \ldots, 20$, using the finite element package COMSOL Multiphysics® 3.5. For simplicity, and without loss of generality, we set $D = 1$ and $\bar{u} = 1$, so that the height of the channel was $a = Pe_a$. The length of the channel was set to 300 units. We used a parabolic flow profile,

$$\mathbf{u}(z) = \frac{3}{2}\left[1 - 4\left(\frac{z}{a}\right)^2\right]\hat{\mathbf{i}} \tag{9}$$

The boundary conditions were constant concentration $c = c_0$ for the upstream wall ($x = 0$), convective flux $\mathbf{n}\cdot\nabla c = 0$ for the downstream wall ($x = 300$), and insulating boundaries $\mathbf{n}\cdot(-D\nabla c + c\,\mathbf{u}) = 0$ for the bottom and top walls ($z = \pm a/2$). Here, $\mathbf{n}$ is the unit normal. The number of triangular mesh elements ranged

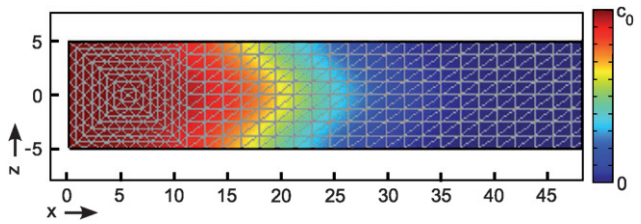

Fig. 7 Example of a finite element simulation. The Péclet number is $Pe_a = 10$ and the time shown is $t = 20$. The gray lines show the finite element grid. Color coding is used to visualize the concentration profile.

from $n = 13952$ for $Pe_a = 2$, down to $n = 2304$ for $Pe_a = 16$. The minimum element quality was

$$q = \frac{4\sqrt{3}A}{h_1^2 + h_2^2 + h_3^2} > 0.8 \qquad (10)$$

where A was the area and h_i were the side lengths of the mesh element. Fig. 7 shows an example of a typical mesh, plotted with a solution of the convection–diffusion equation. For each Pe_a, we analyzed how the concentration on the bottom boundary rises as a function of time, at various downstream distances $x = Pe$. The switching time, defined as the time it takes for the concentration $c(Pe, -Pe_a/2, t)$ to rise from 5% to 95% of its final value, was determined and compared to the predictions of the Taylor–Aris theory. Further numerical analysis besides the finite element simulations was performed with Matlab 7.4 (Mathworks).

7 Acknowledgments

We thank G. Amselem, K. Chang, A. Gholami, W. Pauls, M. Theves, M. Torralba, C. Westendorf, and H. Xu for discussions. C.B. acknowledges support by the Deutsche Forschungsgemeinschaft (SPP 1128).

References

1 H. Andersson and A. van den Berg, Microfluidic devices for cellomics: a review, *Sensors and Actuators B-Chemical*, 2003, **92**(3), 315–325.
2 R. Aris, On the dispersion of a solute in a fluid flowing through a tube, *Proc. Roy. Soc. Lond. A*, 1956, **235**, 67.
3 D. A. Beard, Taylor dispersion of a solute in a microfluidic channel, *J. Appl. Phys.*, 2001, **89**, 4667.
4 D. J. Beebe, G. A. Mensing and G. M. Walker, Physics and applications of microfluidics in biology, *Annual Review of Biomedical Engineering*, 2002, **4**, 261–286.
5 C. Beta, D. Wyatt, W.-J. Rappel and E. Bodenschatz, Flow photolysis for spatiotemporal stimulation of single cells, *Analytical Chemistry*, 2007, **79**, 3940–3944.
6 D. N. Breslauer, P. J. Lee and L. P. Lee, Microfluidics-based systems biology, *Molecular Biosystems*, 2006, **2**(2), 97–112.
7 B. G. Chung, L. A. Flanagan, S. W. Rhee, P. H. Schwartz, A. P. Lee, E. S. Monuki and N. L. Jeon, Human neural stem cell growth and differentiation in a gradient-generating microfluidic device, *Lab Chip*, 2005, **5**, 401–406.
8 J. Dalous, E. Burghardt, A. Müller-Taubenberger, F. Bruckert, G. Gerisch and T. Bretschneider, Reversal of cell polarity and actin-myosin cytoskeleton reorganization under mechanical and chemical stimulation, *Biophys J*, 2008, **94**, 1063–1074.
9 E. Décavé, D. Garrivier, Y. Bréchet, B. Fourcade and F. Bruckert, Shear flow-induced detachment kinetics of *Dictyostelium discoideum* cells from solid substrate, *Biophys J*, 2002, **82**(2383–2395).
10 K. Dorfman and H. Brenner, Comment on "Taylor dispersion of a solute in a microfluidic channel", *J. Appl. Phys.*, 2001, **90**, 6553.
11 M. Etzrodt, H. C. F. Ishikawa, J. Dalous, A. Muller-Taubenberger, T. Bretschneider and G. Gerisch, Time-resolved responses to chemoattractant, characteristic of the front and tall of dictyostelium cells, *Febs Letters*, 2006, **580**(28–29), 6707–6713.
12 J. S. Garanich, R. A. Mathura, Z.-D. Shi and J. M. Tarbell, Effects of fluid shear stress on adventitial fibroblast migration, *Am J Physiol Heart Circ Physiol*, 2007, **292**, H3128.
13 C. L. Hansen, E. Skordalakes, J. M. Berger and S. R. Quake, A robust and scalable microfluidic metering method that allows protein crystal growth by free interface diffusion, *Proceedings of the National Academy of Sciences of the United States of America*, 2002, **99**(26), 16531–16536.
14 P. Herzmark, K. Campbell, F. Wang, K. Wong, H. El-Samad, A. Groisman and H. R. Bourne, Bound attractant at the leading *vs.* the trailing edge determines chemotactic prowess, *Proc. Natl. Acad. Sci.*, 2007, **104**, 13349–13354.
15 D. Irimia, S.-Y. Liu, W. G. Tharp, A. Samadani, M. Toner and M. C. Poznansky, Microfluidic system for measuring neutrophil migratory responses to fast switches of chemical gradients, *Lab Chip*, 2006, **6**, 191–198.
16 N. L. Jeon, H. Baskaran, S. K. W. Dertinger, G. M. Whitesides, L. V. D. Water and M. Toner, Neutrophil chemotaxis in linear and complex gradients of interleukin-8 formed in a microfabricated device, *Nature Biotechnology*, 2002, **20**, 826–830.
17 K. R. King, S. Wang, A. Jayaraman, M. L. Yarmush and M. Toner, Microfluidic flow-encoded switching for parallel control of dynamic cellular microenvironments, *Lab Chip*, 2008, **8**, 107–116.
18 B. Kuczenski, P. R. LeDuc and W. C. Messner, Pressure-driven spatiotemporal control of the laminar flow interface in a microfluidic network, *Lab Chip*, 2007, **7**, 647–649.
19 B. Kuczenski, W. C. Ruder, W. C. Messner and P. R. LeDuc, Probing cellular dynamics with a chemical signal generator, *PLoS ONE*, 2009, **4**, e4847.
20 Y.-S. J. Li, J. H. Haga and S. Chien, Molecular basis of the effects of shear stress on vascular endothelial cells, *Journal of Biomechanics*, 1949, **38**, 2005.
21 J. Liu, M. Enzelberger and S. Quake, A nanoliter rotary device for polymerase chain reaction, *Electrophoresis*, 2002, **23**(10), 1531–1536.
22 J. Olofsson, H. Bridle, J. Sinclair, D. Granfeldt, E. Sahlin and O. Orwar, A chemical waveform synthesizer, *Proc. Natl. Acad. Sci.*, 2005, **102**, 8097–8102.
23 W. Saadi, S.-J. Wang, F. Lin and N. L. Jeon, A parallel-gradient microfluidic chamber for quantitative analysis of breast cancer cell chemotaxis, *Biomedical Microdevices*, 2006, **8**, 109–118.
24 L. Song, S. M. Nadkarni, H. U. Bödeker, C. Beta, A. Bae, C. Franck, W.-J. Rappel, W. F. Loomis and E. Bodenschatz, Dictyostelium discoideum chemotaxis: Threshold for directed motion, *European Journal of Cell Biology*, 2006, **85**, 981–989.
25 L. Soon, G. Mouneimne, J. Segall, J. Wyckoff and J. Condeelis, Description and characterization of a chamber for viewing and quantifying cancer cell chemotaxis, *Cell Motility and the Cytoskeleton*, 2005, **62**, 27–34.
26 S. Takayama, E. Ostuni, P. LeDuc, K. Naruse, D. E. Ingber and G. M. Whitesides, Laminar flows - subcellular positioning of small molecules, *Nature*, 2001, **411**(6841), 1016–1016.
27 G. Taylor, Dispersion of soluble matter in solvent flowing slowly through a tube, *Proc. Roy. Soc. Lond. A*, 1953, **219**, 186.
28 T. Thorsen, S. J. Maerkl and S. R. Quake, Microfluidic large-scale integration, *Science*, 2002, **298**(5593), 580–584.
29 G. M. Whitesides, E. Ostuni, S. Takayama, X. Y. Jiang and D. E. Ingber, Soft lithography in biology and biochemistry, *Annual Review of Biomedical Engineering*, 2001, **3**, 335–373.
30 D. Wyatt, Chemotaxis in microfluid channels, *PhD dissertation, Cornell University*, 2007.